International Journal of Heat and Technology
Vol. 41, No. 3, June, 2023, pp. 498-512
Journal homepage: http://iieta.org/journals/ijht

Thermal Circuit Analysis and Performance Evaluation of Evaporative Cooling Transformers Within Advanced Industrial Logistics Infrastructure

Hualin Shi[1,2*], Bin Xiong[2,3], Kangjie Huang[2,3], Yiwei Ding[2,3], Guobiao Gu[2,3]

[1] Huayuan International Land Port Group Co., Ltd, Shanxi 030021, China
[2] Institute of Electrical Engineering Chinese Academy of Sciences, Beijing 100190, China
[3] School of Electronic Electrical and Communication Engineering, University of Chinese Academy of Sciences, Beijing 100049, China

Corresponding Author Email: shihualin18@mails.ucas.ac.cn

https://doi.org/10.18280/ijht.410303

Received: 28 June 2022
Accepted: 25 April 2023

Keywords:
evaporative cooling technology, thermal circuit model, transformer

ABSTRACT

The progressive trend towards intelligent, eco-friendly, low-carbon, and sustainable development in contemporary industrial logistics parks has catalyzed a substantial influx of new energy power systems. This integration poses unique challenges, including intermittent and fluctuating load characteristics, due to the operation of high-powered machinery such as belt conveyors. Consequently, traditional distribution transformers often face premature failure, attributed primarily to inadequate overload capacity, thereby compromising grid safety. Evaporative cooling technology, as a countermeasure to these thermal constraints, holds the potential to enhance the heat dissipation capacity, thus mitigating overload issues. This study employs a novel methodological blend of thermal circuit parameter analysis and empirical experimentation to comprehensively investigate the performance attributes of evaporative cooling distribution transformers. This study's innovative approach involves the development of a dynamic piecewise thermal circuit model that encapsulates both the natural convection and nucleate boiling heat transfer stages. This model builds on the intrinsic attributes of the pool boiling curve of a low-boiling-point coolant. Critical aspects under scrutiny include thermal circuit parameters, boiling heat transfer correlations, constraints on critical heat flux density, and characteristics of the evaporative coolant. Following the Rohsenow correlation and model experimentation, a suitable boiling heat transfer correlation for the selected evaporative coolant was formulated. The thermal circuit model was then employed to discern the influence of the load coefficient, ambient temperature, and coolant boiling point on the operational behavior of the evaporative cooling transformer. The analysis revealed that evaporative cooling transformers exhibit a commendable aptitude for handling impact, intermittent, and fluctuating loads, demonstrating substantial overload resistance. Hence, they are favorably poised for extensive application in heavy-load industrial logistics parks, especially those harnessing new energy. These findings provide instrumental insights, potentially propelling advancements in the modern industrial logistics landscape.

1. INTRODUCTION

In response to escalating climate concerns, the consensus has coalesced globally around carbon reduction, positioning new energy as a viable mitigation strategy. This policy has fostered a significant integration of new energy power generation systems, including wind and solar energy, into industrial logistics parks. However, the intermittent and fluctuating nature of new energy electricity (as illustrated in Figure 1) frequently exposes the connecting transformer to overload conditions, posing a considerable threat to grid safety [1].

Common oil-immersed transformers typically use mineral oil as coolant. Despite its flammability, low lightning, and non-biodegradable nature falling short of safety and environmental standards, such transformers persist. As a remedy, dry transformers are predominantly employed in modern industrial logistics parks. Yet, dry transformers also present limitations. Air, their primary insulating and coolant agent, yields lower insulation and heat capacity than transformer oil. Consequently, their cooling efficiency is compromised, resulting in larger volume, increased weight, reduced overload energy, and inferior operational performance and economy compared to oil-immersed transformers of equivalent capacity. Manufacturing such transformers with large capacities remains challenging.

Industrial logistics parks often contain high-power equipment such as belt conveyors, hoists, and water pumps, characterized by high starting currents and long durations. These assets are prone to overloads and frequent starts, potentially blocking the rotor in operation, thereby inducing impulsive loads (as shown in Figure 2) that can cause short-term transformer overloads.

Effectively, transformer overload within industrial logistics parks can be ascribed to inadequate heat dissipation. Evaporative cooling technology, which reinforces heat dissipation, has been investigated as a potential solution for these thermal issues. This technology employs a fluorocarbon

coolant to absorb latent heat from heated components, enabling thermal system self-circulation [2]. Its merits of power insulation, excellent cooling performance, low system pressure, ease of maintenance, simple operation, non-flammability, safety, and reliability have facilitated its successful application in a range of electrical equipment, including hydroelectric generators (such as two 700MW units in the Three Gorges) [3], steam turbine generators [4], iron separators [5], frequency converters [6, 7], ion source magnets [8], and supercomputers [9, 10].

Despite these advances, there is limited research on evaporative cooling transformers, particularly distribution transformers below 35kV. Laboratory high-pressure breakdown experiments have indicated that evaporative coolants below 35kV meet transformer insulation requirements [11]. As an efficient, environmentally friendly, non-flammable, and non-explosive cooling technology, it has the technical potential to address the prevalent thermal issues in distribution transformers within industrial logistics parks. This study will explore the principles of this technology, combine experimental analysis with thermal circuit, provide experimental verification, and perform a performance analysis based on thermal circuit models.

(a) New energy power generation equipment

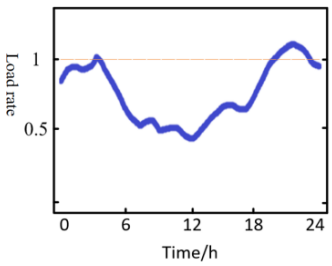

(b) Load curve of wind energy

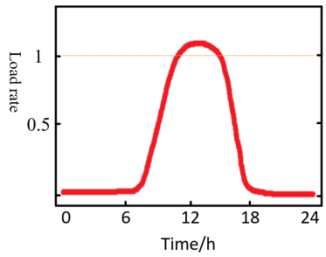

(c) Load curve of solar energy

Figure 1. Typical load curve of new energy power generation and transformer

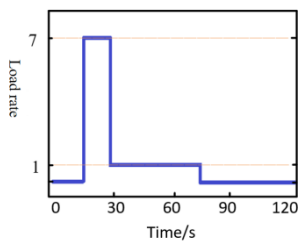

Figure 2. Typical impact load characteristic curve

2. MECHANISM AND OPTIMISATION OF EVAPORATIVE COOLING TRANSFORMERS

The transformer utilises the method of immersed self-circulation evaporative cooling. This method immerses the transformer's core and coil in a fluorocarbon evaporative coolant that possesses a suitable boiling point, fulfils insulation requirements, demonstrates efficient heat transfer and is noncombustible. This coolant undergoes a liquid-vapour phase transition to absorb latent heat, providing greater heat dissipation efficiency than the conventional method relying on natural convection of the casing.

The schematic representation of submerged evaporative cooling in transformers is portrayed in Figure 3. Heat loss initiated from the transformer coil is first transferred to the outer surface of the insulating paper via heat conduction. Following this, convective heat transfer with the evaporative coolant ensues. The coolant then absorbs the heat, instigating a partial vaporisation. This latent heat is rapidly stored within the boiling, vaporised bubbles. Owing to the buoyancy created by density variations, the vaporous coolant ascends, reaching the condenser through the steam pipe for secondary heat exchange. Post-release of the latent heat, the coolant reverts to its liquid state, then flows back into the casing along the liquid pipe due to gravity. This process engenders a self-circulating thermal system.

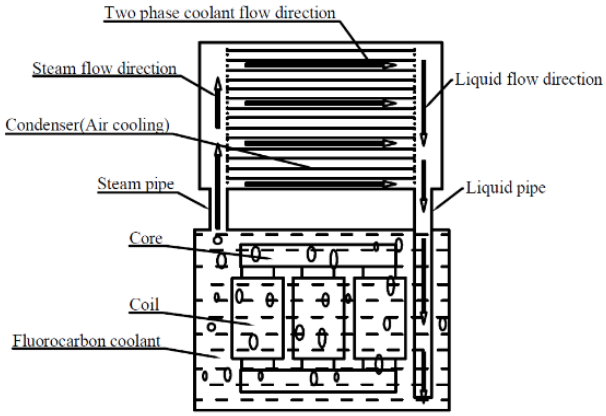

Figure 3. Schematic diagram of transformer submerged evaporative cooling

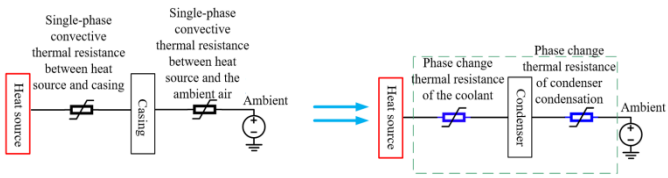

Figure 4. Optimisation path for thermal resistance of evaporative cooling transformer

Through an analysis of the thermal circuit parameters of traditional distribution transformers, it is discerned that the transformer's heat issue can be traced back to the internal and external thermal circuit convective heat resistance. Immersed evaporative cooling optimises the single-phase convective thermal resistance of the transformer's internal thermal circuit to a boiling phase change thermal resistance. Concurrently, the single-phase convective thermal resistance of the external thermal circuit to air is optimised to a condensing phase

change thermal resistance via the condenser. As phase change thermal resistance is substantially lower than single-phase convective thermal resistance, this considerably diminishes the transformer's internal and external thermal resistance. This process effectively optimises the transformer's thermal circuit, as visualised in Figure 4.

3. ANALYSIS OF THE THERMAL CIRCUIT IN EVAPORATIVE COOLING TRANSFORMERS

In transformers, replacing the traditional transformer oil with a low boiling point, low viscosity evaporative coolant optimizes the single-phase convective heat transfer thermal resistance to a convective heat transfer thermal resistance based on phase change principles. The static liquid boiling formed through the internal submerged solid interface or outer wall, known as pool boiling, can be attributed to the heat transfer process of the large container pool in transformers that utilize immersion evaporative cooling. It is accepted that the heat flux density, inclusive of convective heat transfer coefficient or phase change thermal resistance, correlates with the difference between the heater surface temperature (Tw) and the coolant liquid saturation temperature (Ts) or the degree of superheat [12].

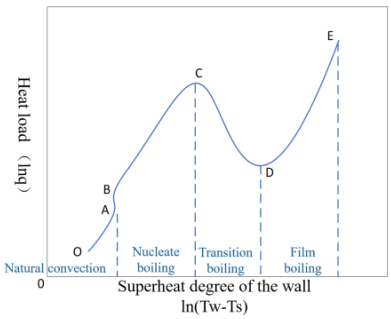

Figure 5. Low boiling point coolant pool boiling curve

Assuming the temperature distribution on the transformer coil and core surface under the evaporative cooling optimization mode is uniform, the complexity of the boiling phase change heat transfer process is appreciated. Existing research on boiling heat transfer relies on Nukiyama's boiling curve [12], which identifies variables affecting pool boiling heat transfer and offers significant insights for the parameter analysis of the thermal circuit model. The boiling heat transfer experimental curve of low boiling point organic coolant R12, which is presented in Figure 5 [13], illuminates the relationship between heat flux density (heat load) and the degree of superheat, highlighting the stages of natural convection, nuclear boiling, and film boiling.

3.1 Thermal circuit model: Natural convection phase

The initial heating stage, as illustrated in the OA section of Figure 5, presents a low degree of superheat on the heater surface with virtually no bubble generation. Here, heat is primarily transferred from the heating surface to the mainstream area or liquid-vapor interface via single-phase natural convection heat transfer. This is articulated in Eqs. (1)-(3).

$$\frac{h_{l-\mathrm{cov}} l_{h-tz}}{\lambda_l} = 0.59\left[\left(\frac{g\Delta\theta_{w-l}\alpha_l l_{h-tz}^3 \rho_l^2}{\mu_l^n}\right)\left(\frac{C_{p-l}\mu_l}{\lambda_l}\right) \right]^{0.25} \tag{1}$$

where, $l_{h\text{-}tz}$ and $\Delta\theta_{w\text{-}l}$ represent the characteristic size of the heating body and the difference between the liquid saturation temperature of the heating body surface and the coolant, respectively. On the other hand, $h_{l\text{-}cov}$, λ_l, α_l, $C_{p\text{-}l}$, μ_l correspond to the convective heat transfer coefficient, thermal conductivity coefficient, thermal expansion coefficient, constant pressure specific heat capacity, and dynamic viscosity of the liquid coolant.

Considering a constant heat flux density and the Newtonian cooling equation:

$$q = h_{l-\mathrm{cov}}(\theta_w - \theta_l) \tag{2}$$

Eqs. (1) and (2) collectively yield the single-phase convection heat transfer coefficient between the coolant and the surface of the heating body and the average surface temperature of the heating body. The thermal resistance is then obtained by Eq. (3).

$$R_{th-l-\mathrm{cov}} = \frac{1}{h_{l-\mathrm{cov}} A_h} \tag{3}$$

where, A_h signifies the heat transfer area of the heating body while $R_{th\text{-}l\text{-}cov}$ represents the convective heat transfer thermal resistance between the heat sources and the cooling medium. This corresponds to the convective heat transfer thermal resistance of the low-voltage coil, high-voltage coil, oil tank inner wall, and working medium, indicated respectively as $R_{th\text{-}LV\text{-}clt}$, $R_{th\text{-}HV\text{-}clt}$, $R_{th\text{-}clt\text{-}tank}$.

To account for the impact of the flow channel, the high and low voltage coil and the core are considered three independent heat sources, leading to the thermal circuit model of the natural convection stage as shown in Figure 6.

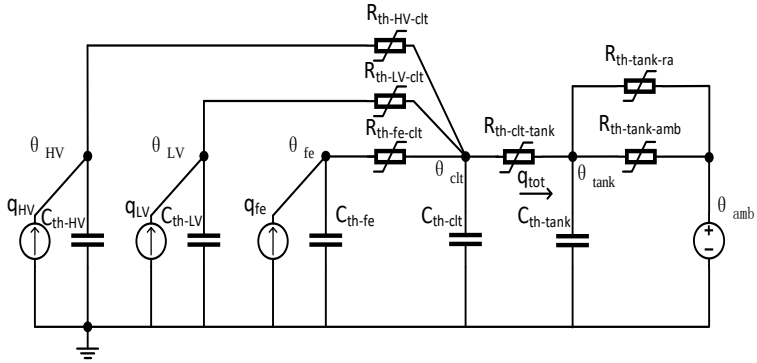

Figure 6. Natural convection thermal circuit model of evaporative cooling transformer

The differential equation system is:

$$\begin{cases} C_{th-HV}\dfrac{d\theta_{HV}}{dt} = K^2 q_{HV.R} - \dfrac{\theta_{HV}-\theta_{clt}}{\mathrm{R}_{\text{th-HV-clt}}} \\ C_{th-LV}\dfrac{d\theta_{LV}}{dt} = K^2 q_{LV.R} - \dfrac{\theta_{LV}-\theta_{clt}}{\mathrm{R}_{\text{th-LV-clt}}} \\ C_{th-fe}\dfrac{d\theta_{fe}}{dt} = q_{fe} - \dfrac{\theta_{fe}\text{-}\theta_{clt}}{\mathrm{R}_{\text{th-fe-clt}}} \\ C_{th-clt}\dfrac{d\theta_{clt}}{dt} = \dfrac{\theta_{HV}-\theta_{clt}}{\mathrm{R}_{\text{th-HV-clt}}} + \dfrac{\theta_{LV}-\theta_{clt}}{\mathrm{R}_{\text{th-LV-clt}}} + \dfrac{\theta_{fe}\text{-}\theta_{clt}}{\mathrm{R}_{\text{th-fe-clt}}} - \dfrac{\theta_{clt}-\theta_{\tan k}}{\mathrm{R}_{\text{th-clt-tank}}} \\ C_{th-\tan k}\dfrac{d\theta_{\tan k}}{dt} = \dfrac{\theta_{clt}-\theta_{\tan k}}{\mathrm{R}_{\text{th-clt-tank}}} - \dfrac{\theta_{\tan k}-\theta_{\text{amb}}}{\mathrm{R}_{\text{th-tank-amb}}} - \dfrac{\theta_{\tan k}-\theta_{\text{amb}}}{\mathrm{R}_{\text{th-tank-ra}}} \end{cases} \tag{4}$$

3.2 Characteristics of thermal circuit and boiling heat transfer in the nucleate state

As depicted in Figure 6, the pool boiling curve of low boiling point initiates at point A, subsequently producing an increasing number of bubbles on the surface of the heated entity. The intensity of boiling heat transfer surpasses that of the single-phase convective heat transfer, and the superheat degree rapidly attains point B after a brief decrement phase. This period is designated as the nascent phase of nucleate boiling, also referred to as bubble boiling.

Transitioning into the BC phase, the state of complete nucleate boiling is entered. Rohsenow postulated that the heat transfer mechanism in the nucleate boiling process is triggered when bubbles disengage from the heating body's surface, inciting a violent disruption in the boundary layer of the liquid and substantially augmenting the surface heat transfer coefficient [14]. It has been observed from research findings on the heat transfer mechanism of liquid nucleate boiling that heat transfer efficiency is influenced by several parameters including the rate of bubble production, the size of the bubble, and the degree to which the fluid submerges the heating body surface. It is a function of the flow parameters and physical property parameters. Thus, appropriate criteria must be identified to describe the heat transfer characteristics of pool boiling.

Enhancing nucleate boiling heat transfer fundamentally depends on the location where the bubble core is formed. Studies indicate that features like grooves and cracks on the heating surface can be readily converted into vaporization cores. The prerequisites for steam bubble formation are as follows:

$$R_b = \frac{2\sigma}{p_v - p_s} \tag{5}$$

where, σ denotes the surface tension at the bubble-liquid interface, p_v signifies the steam pressure in the bubble, and p_s is the saturated pressure of the boiling system.

Based on the principle of bubble force balance, a certain degree of superheat, θ_l-θ_s, is required for the vaporization core. This implies that the liquid temperature, θl, outside the bubble in the boiling state must exceed the corresponding saturation temperature, θs, under the system pressure. It becomes evident that the degree of superheat is an essential parameter pertaining to nucleate boiling. The relationship between the superheat degree, θ_l-θ_s, and bubble radius, R_b, can be determined by the Clansius-Clapeyron equation as follows:

$$\theta_l - \theta_s = \frac{2\sigma}{r\rho_v R_b} \tag{6}$$

where, r symbolizes the latent heat of the coolant liquid vaporization, ρ_v signifies the steam density in the bubble. It must be noted that the liquid temperature outside the bubble, θ_l, aligns with the temperature on the heating element surface, θ_w.

The complex behavior of bubbles results in the mutual transfer of heat, mass, and momentum among the liquid, solid, and vapor states in the pool boiling process. Various factors such as the physical parameters of the coolant, surface condition of the heating body among others, exert influence on the heat transfer performance. Therefore, deriving a mathematical analytical expression of boiling heat transfer with nonlinear physical characteristics is challenging, similar to single-phase heat transfer. Among researchers, there is a significant divergence in the calculation formula for saturated nucleate boiling in large containers.

For example, the W. Rohsenow formula [14], extensively employed as a working fluid, was formulated by W.Rohsenow utilizing the natural convection criterion method to procure the corresponding criterion function. Nu_b、Re_b and Pr_l are utilized as three criterion numbers to represent the nucleate boiling heat transfer capacity, the rate of bubble production, and parameters associated with the physical properties of the fluid coolant. Generally, the natural convection criterion formula is expressed as follows:

$$\frac{Re_b Pr_l}{Nu_b} = C_b Re_b^{m1} Pr_l^{n1} \tag{7}$$

A substantial contributor to enhanced convective heat transfer is the persistent generation and liberation of bubbles from the heating element's surface. The Re_b number representing bubble motion is expressed by the following relation:

$$Re_b = \frac{\mathrm{G_b D_b}}{\mu_l} \tag{8}$$

where, μ_l denotes liquid viscosity, G_b signifies the mass flow rate of bubble detachment from the heating body surface, and D_b is the diameter at which the bubble detaches. The parameters are further defined by:

$$\mathrm{G_b} = \frac{\pi}{6}\mathrm{fnD_b^3}\rho_v \tag{9}$$

where, f is the frequency at which the bubble detaches from the heating surface. As two significant parameters in bubble dynamics, f and D_b are intimately linked with the mechanism of nucleate boiling heat transfer. These parameters constitute areas of intense scholarly interest both domestically and internationally [15].

Based on the equilibrium theory of bubble buoyancy and vapor-liquid surface tension, Fritz proposed an empirical formula to calculate bubble separation diameter D_b. The formula correlates D_b with the surface tension σ at the bubble-liquid interface, the contact angle Ψ between the steam bubble and heating element surface, and the densities of saturated vapor ρv and saturated liquid ρ_l.

$$D_b = 0.0208\psi\sqrt{\frac{\sigma}{g(\rho_l - \rho_v)}} \tag{10}$$

The Nu_b number is then calculated using the following relation:

$$Nu_b = \frac{qD_b}{(\theta_w - \theta_s)\lambda_l} \tag{11}$$

From Eqs. (5) to (11), W. Rohsenow synthesized with experimental data analysis to derive the dimensionless criterion formula for nucleate boiling heat transfer:

$$\frac{C_{p-l}(\theta_w - \theta_s)}{r} = C_{wl}\left[\frac{q}{\mu_l r}\sqrt{\frac{\sigma}{g(\rho_l - \rho_v)}}\right]^{m1}\left[\frac{C_{p-l}\mu_l}{\lambda_l}\right]^{n1} \tag{12}$$

where, C_{p-l} denotes the constant pressure specific heat capacity of the saturated liquid coolant, C_{wl} represents the constant associated with the wet thermal surface of the coolant, m1 is typically set to 0.33 based on experimental findings, and n1 denotes an empirical constant associated with the surface of the heating body and the type of coolant.

Boiling heat transfer correlations for evaporative cooling fluorocarbon coolants have been scarcely reported internationally. In China, principal experimental investigations have been conducted by the Institute of Electrical Engineering, Chinese Academy of Sciences and Hebei University of Technology. Chen Zhenbin conducted an investigation on the boiling heat transfer coefficient of a fully immersed evaporative cooling motor with a box structure, with bare copper wire and varying insulating materials. It was found that insulating the coil does not necessarily diminish heat transfer performance by separating the cooling medium from the heating body's surface. On the contrary, some capillary insulating materials were shown to enhance the vaporization core, reduce the diameter of bubble detachment, increase the rate of bubble formation, thereby augmenting boiling heat transfer and improving the boiling heat transfer coefficient [16].

Bare copper wire surfaces were evaluated using Eq. (13), white ribbon-wrapped wires with Eq. (14), and glass ribbon-wrapped wires with Eq. (15).

$$h_{ft} = 5.94q_{\_rlmd}^{0.652} \text{ (For the bare copper wire surfaces)} \tag{13}$$

$$h_{ft} = 8.39q_{\_rlmd}^{0.652} \text{ (For wire wrapped with White ribbon)} \tag{14}$$

$$h_{ft} = 15.29q_{\_rlmd}^{0.652} \text{ (For wire wrapping with glass ribbon)} \tag{15}$$

Luan Ru, through rigorous analysis and processing of nearly ten thousand experimental data points, derived boiling heat transfer correlations between r113 evaporative cooling coolant and motor coil and stator core in narrow spaces, respectively. These correlations were incorporated into formulae and pressure factors were included [17]. Eq. (16) was employed for a 6mm narrow channel between core and coolant, while Eq. (17) was used for a 6mm narrow channel between coil and coolant, where $\frac{p}{p_0}$ represents relative pressure. It must be noted that the heat flux density unit qb is W/mm^2.

$$h_{ft} = q_b^{0.752}\left(0.866 + 2.56\left(\frac{p}{p_0}\right)\right) \tag{16}$$

$$h_{ft} = q_b^{0.75}\left(0.556 + 1.94\left(\frac{p}{p_0}\right)\right) \tag{17}$$

Based on empirical data obtained from a prototype model of an evaporative cooling transformer, Deng Bo devised a re-fitted index of the superheat degree. This prototype, constructed according to the electromagnetic scheme of a 30kVA oil transformer, utilized r113 as the evaporative cooling medium. The resulting empirical correlation formula signifies the relationship between heat flux density and superheat degree as follows [18]:

$$q_{\_rlmd} = 6664\Delta\theta_{w-s}^{1.41} \tag{18}$$

Cooper's formula, widely recognized in the field of refrigeration working medium, was applied by Song Mingkai for direct computation of the boiling heat transfer coefficient of a fully immersed evaporative cooling transformer. A relational expression [19] linking the boiling heat transfer coefficient, heat flux density, and superheat was subsequently fitted, corresponding to varied heating power values, as shown below:

$$h_{ft} = q_{\_rlmd}^{-0.62103\Delta\theta+1.37131} \tag{19}$$

Zhao Wei and Zhang Chunqiao directly utilized the W. Rohsenow formula to compute the boiling heat transfer coefficient of the evaporative cooling transformer. In these computations, Zhao Wei assigned a value of 0.77 to n1 for the r113 coolant [20-22].

In mathematical representation, the boiling heat transfer correlation embodies the relationship between the boiling heat transfer coefficient (or superheat degree) and heat flux density. This correlation can be reconfigured into the relation between the boiling heat transfer coefficient and heat flux density on the heating body's surface via the transformation of thermal circuit parameters. Consequently, the correlation equation for boiling heat transfer parameters can be mathematically expressed as follows:

$$h_{ft} = C_{ft}q_{\_rlmd}^{m2} \tag{20}$$

where, C_{ft} and m^2 represent constant parameter terms.

The complexity of pressure influence factors mandates that experimental studies on nucleate boiling heat transfer coefficients be conducted under constant pressure, emphasizing the relationship with heat flux density. W. Rohsenow's correlation formula, premised on boiling heat transfer performance, bubble generation, and coolant's physical property parameters, incorporates criteria such as Nu_b, Re_b, and Pr_l. A theoretically sounder representation of boiling heat transfer correlation is achieved by using these criteria. Therefore, the present study examines the boiling heat transfer coefficient of the chosen evaporative coolant grounded on the W. Rohsenow correlation, with experimental modification of

C_{wl} and n^1 parameters.

3.3 Critical heat flux density limitations

As presented in Figure 6, the maximum heat flux peak value (q_{CHF}) of nucleate boiling is observed at point C, also known as the critical heat flux (CHF). Subsequent increases in superheat degree progressively form a vapor film covering portions of the heating surface area. An unstable transition boiling stage ensues, characterized by a gradual decrease in heat flux density with increasing superheat degree, until reaching the minimum heat flux density at point D. This point, referred to as the Leidenfrost point, delineates the boundary between transition boiling and stable film boiling. From this point, a stable film boiling stage commences wherein generated steam bubbles entirely cover the heating surface, creating a vapor film layered region. This region acts like a larger vapor film thermal resistance link in the heat transfer path, thereby degrading the heat transfer performance. Thus, it is imperative to maintain the heat source's heat flux density beneath the critical heat flux density (q_{CHF}).

Zuber's formula [12, 13], utilized for calculating the critical heat flux density of infinite space pool boiling (with a horizontal flat plate heating surface), is adopted for q_{CHF} calculation:

$$q_{CHF-\inf} = 0.149 r \rho_v^{0.5} [\sigma g(\rho_l - \rho_v)]^{0.25} \tag{21}$$

In instances of varied shaped heating surfaces in restricted space, a correction coefficient f (L ') [23] is added, yielding the critical heat flux density of finite space:

$$q_{CHF} = q_{CHF-\inf} f(L') \tag{22}$$

where,

$$L' = \frac{L}{\sqrt{\sigma[g(\rho_l - \rho_g)]}} = 2\pi \frac{\sqrt{3} L_{\min}}{\lambda_d} \tag{23}$$

where, L_{min} signifies the minimum feature size, for example, the radius, thickness, width, etc.

When considering the transformer's coil and core as cylindrical, the correction coefficient of the cylinder becomes:

Horizontal cylinder (L'> 0.15):

$$f(L') = 0.89 + 2.27 \exp(-3.44 R^{0.5}) \tag{24}$$

For the horizontal heating surface under large horizontal cylinder (L'>1.2) and small horizontal cylinder (0.15<L'<1.2) configurations, $f(L')$ is 0.9 and 0.94L' $^{-0.25}$ respectively. In the case of vertical heating surfaces, a correction factor of 0.75 is applied.

Given the low-voltage coil's small number of turns and smaller heating surface than the high-voltage coil, the flow channel's configuration must ensure the heating surface area retains the heat source's heat flux density beneath q_{CHF} under all overload conditions. The heat loss and heating surface area of the low-voltage coil should conform to Eq. (25):

$$\frac{q_{LV}}{A_{LV-clt}} < q_{CHF} \tag{25}$$

Applying Eq. (25) and in consideration of the single-phase experimental model, the critical heat flux density was computed to be 66096W/m^2. However, the calculated heat flux density under the maximum overload condition (K=7 impact load) studied in this work was found to be less than 5000W/m^2. Consequently, the heat flux density of boiling heat transfer investigated was exceptionally low, situated at the nucleate boiling curve's initial stage, wholly conforming to the critical heat flux density's limit requirements.

3.4 Thermal circuit model development in the nucleate boiling phase

Despite the AB stage at the onset of nucleate boiling exhibiting variations from both the natural convection stage (OA) and the complete nucleate boiling stage (BC), the short-lived and minor influence of the AB stage facilitates its classification under nucleate boiling. Consequently, the AB stage and BC stage are collectively analyzed within a unified nucleate boiling thermal circuit model.

Eq. (20), representing the boiling heat transfer experimental correlation, can also be restructured into a correlation between superheat degree and heat flux density:

$$\theta_w - \theta_s = \frac{q_{\_rlmd}^{1-m2}}{C_{ft}} \tag{26}$$

Eq. (26) indicates that the surface temperature of the heat source relates solely to the saturation temperature θs, heat flux density $q_{\_rlmd}$, and parameters C_{ft}, all under the pressure of the boiling system. Thus, in the thermal circuit model's construction, it is presumed that the system possesses comprehensive matching condensation capacity. The condensation parameter and the shell's heat dissipation are reasonably dismissed. The boiling system pressure p_s of the evaporative coolant corresponds to θ_s and serves as the boiling point $\theta_{clt\text{-}bp}$ of the evaporative cooling coolant at this pressure, which can thus be expressed as a function f(p) of absolute pressure p.

The variation in heat flux density across the three heat sources might lead to dissimilar heat transfer stages due to temperature differences at the coil's heating surface and nearby working medium. Whether the node temperature θclt of the evaporative coolant in the thermal circuit attains the boiling point temperature $\theta_{clt\text{-}bp}$, and whether the superheat degree between the heating surface and coolant reaches the nucleate boiling threshold value Δs, can serve as combined criteria for distinguishing different heat transfer stages of natural convection and nucleate boiling. A heat source surface in the nucleate boiling stage is identified by the temperature θ_{clt} of the evaporative coolant reaching the boiling point temperature and the superheat degree of the heating surface attaining the nucleate boiling threshold value Δs; otherwise, it is categorized in the natural convection stage. Combining the varied temperature conditions of the core, high and low voltage coils could lead to the formation of multiple heat transfer criteria combinations.

An analysis of several typical operational conditions based on whether the temperature θ_{clt} of the evaporative coolant attains the boiling point temperature $\theta_{clt\text{-}bp}$ follows.

(1) The temperature θclt of the evaporative coolant has not reached the boiling point temperature $\theta_{clt\text{-}bp}$.

In this scenario, the core, high and low voltage coils are within the natural heat transfer stage. The corresponding thermal circuit model is depicted in Figure 6.

(2) The boiling point temperature θclt-bp is reached by the evaporative coolant temperature θ_{clt}.

The corresponding thermal circuit model is provided in Figure 7 under this condition, illustrating the boiling heat transfer thermal circuit model 1 of the evaporative cooling transformer.

In the event that the superheat degree of the heat source does not satisfy the nucleate boiling threshold, it is conceivable that all three heat sources are in the natural convection heat transfer stage. This is visualized in the heat path model as depicted in Figure 6. As the heat flux density of the low-voltage coil exceeds that of the high-voltage coil and the core, an increase in temperature is likely to first cause the superheat degree of the low-voltage coil's heating surface to reach the nucleate boiling threshold value Δs. This implies that the low-voltage coil should ideally be the first to enter the nucleate boiling heat transfer stage. The corresponding thermal circuit model is provided in Figure 7.

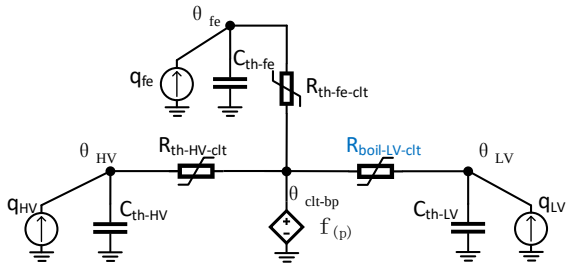

Figure 7. Boiling heat transfer thermal circuit model 1 of evaporative cooling transformer

Under such conditions, the low-voltage coil exists in the nucleate boiling stage, while the high-voltage coil and iron core are in the natural convection stage. The corresponding node differential equations are given in Eq. (27). The thermal circuit model suggests that once the coolant temperature achieves the boiling point, the heat flux of the heat source is entirely correlated with the boiling point temperature $\theta_{clt\text{-}bp}$ of the coolant. This model disregards the natural convection heat transfer portion of the tank shell and assumes that the condenser performance entirely fulfills the condensation requirements.

The differential equations of the corresponding nodes are:

$$\begin{cases} C_{th-HV}\dfrac{d\theta_{HV}}{dt} = K^2 q_{HV.R} - \dfrac{\theta_{HV}-\theta_{clt-bp}}{\mathrm{R}_{\text{th-HV-clt}}} \\ C_{th-LV}\dfrac{d\theta_{LV}}{dt} = K^2 q_{LV.R} - \dfrac{\theta_{LV}-\theta_{clt-bp}}{\mathrm{R}_{\text{boil-LV-clt}}} \\ C_{th-fe}\dfrac{d\theta_{fe}}{dt} = q_{fe} - \dfrac{\theta_{fe}\text{-}\theta_{clt-bp}}{\mathrm{R}_{\text{th-fe-clt}}} \\ \theta_{clt-bp} = f(p) \end{cases} \tag{27}$$

Additionally, thermal circuit models wherein only the high and low voltage coil meet the nucleate boiling conditions, and all three heat sources meet the nucleate boiling conditions, are provided in Figures 8 and 9 respectively. In Figure 8, both high and low voltage coils are in nucleate boiling, and the core is in the natural convection stage. Figure 9 presents a situation where all three heat sources are in the nucleate boiling stage. Several combinations of these criteria should be represented in the thermal circuit program.

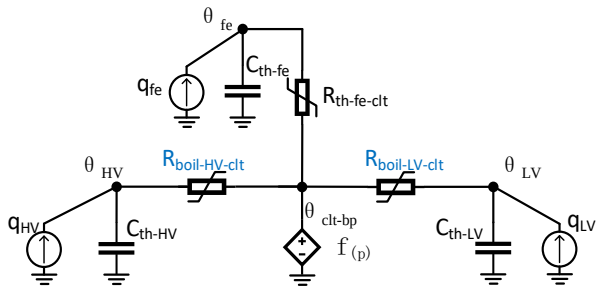

Figure 8. Boiling heat transfer thermal circuit model 2 of evaporative cooling transformer

Figure 8 represents the boiling heat transfer thermal circuit model 2 of the evaporative cooling transformer, with the differential equations of the corresponding nodes as follows:

$$\begin{cases} C_{th-HV}\dfrac{d\theta_{HV}}{dt} = K^2 q_{HV.R} - \dfrac{\theta_{HV}-\theta_{clt-bp}}{\mathrm{R}_{\text{boil-HV-clt}}} \\ C_{th-LV}\dfrac{d\theta_{LV}}{dt} = K^2 q_{LV.R} - \dfrac{\theta_{LV}-\theta_{clt-bp}}{\mathrm{R}_{\text{boil-LV-clt}}} \\ C_{th-fe}\dfrac{d\theta_{fe}}{dt} = q_{fe} - \dfrac{\theta_{fe}\text{-}\theta_{clt-bp}}{\mathrm{R}_{\text{th-fe-clt}}} \\ \theta_{clt-bp} = f(P) \end{cases} \tag{28}$$

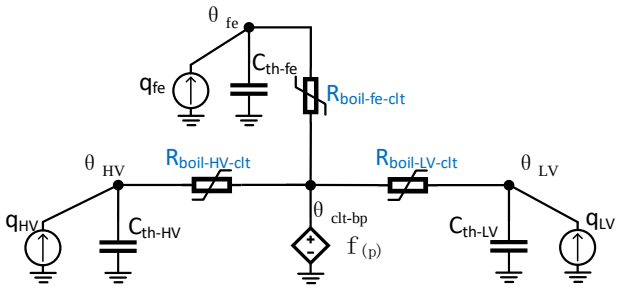

Figure 9. Boiling heat transfer thermal circuit model 3 of evaporative cooling transformer

Figure 9 demonstrates the boiling heat transfer thermal circuit model 3 of the evaporative cooling transformer, with the differential equations of the corresponding nodes:

$$\begin{cases} C_{th-HV}\dfrac{d\theta_{HV}}{dt} = K^2 q_{HV.R} - \dfrac{\theta_{HV}-\theta_{clt-bp}}{\mathrm{R}_{\text{boil-HV-clt}}} \\ C_{th-LV}\dfrac{d\theta_{LV}}{dt} = K^2 q_{LV.R} - \dfrac{\theta_{LV}-\theta_{clt-bp}}{\mathrm{R}_{\text{boil-LV-clt}}} \\ C_{th-fe}\dfrac{d\theta_{fe}}{dt} = q_{fe} - \dfrac{\theta_{fe}\text{-}\theta_{clt-bp}}{\mathrm{R}_{\text{boil-fe-clt}}} \\ \theta_{clt-bp} = f(P) \end{cases} \tag{29}$$

where, the subscript 'th' signifies the single-phase convective heat transfer thermal resistance, while the subscript 'boil' indicates the boiling heat transfer thermal resistance.

The coil is entirely submerged in the evaporative cooling medium, with θ_{LV} representing the outer surface temperature

of the low-voltage winding. The effective heat absorption capacity, efficient thermal conductivity, low flow resistance, and low viscosity of two-phase boiling of the evaporative cooling working fluid can ensure surface temperature uniformity of the heat-generating body [7]. Therefore, it can be postulated that the temperature of the low-voltage coil is uniform, and the temperature θ_{LV} of the low-voltage coil is considered a hot spot temperature.

4. EXPERIMENTAL STUDY AND VERIFICATION OF THERMAL CIRCUIT MODEL

4.1 Experimental system and device

The experimental system and corresponding device utilized in this study are graphically represented in Figure 10 and Figure 11. These illustrations incorporate a transformer box model, core, single-phase high and low voltage coils, condensers, and Polyurethane (PU) pipes that serve as the steam collection and return conduits for coolant circulation. Activation of the high and low voltage coils in the model box via a high-power supply results in load loss which functions as a heat source, warming the evaporative coolant housed in the box. Upon reaching the saturation temperature relative to the prevailing pressure, the coolant initiates the absorption of latent heat for vaporization.

The steam-liquid working medium, owing to the density difference, generates a dynamic pressure head. The steam coolant, carrying the latent heat, is transferred from the box to the upper air condenser through the steam pipe. Inside the condenser, the steam coolant relinquishes the latent heat and condenses into a liquid state. It then returns to the box via the liquid pipe due to the force of gravity, thus completing a pump-free self-circulation cooling process of the coolant and maximizing energy efficiency of the cooling system.

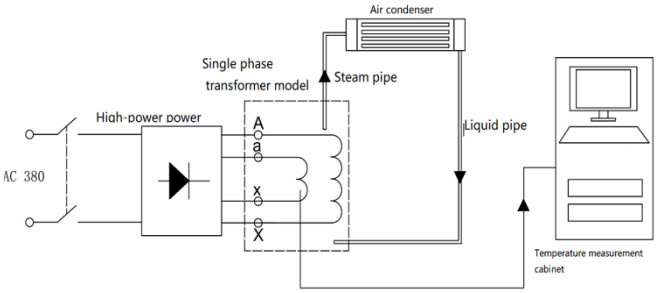

Figure 10. Schematic diagram of experimental system

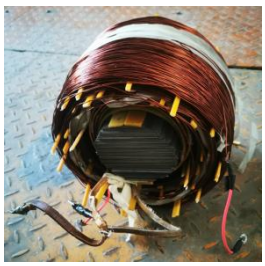

Figure 11. Coil and core structure

The structure of the single-phase coil core is detailed in Figure 11. A flow channel is present between the coil, and a PT100 temperature probe is assigned for the high and low voltage coil and insulation cylinder. The maximum temperature value at the measuring point is denoted as the experimental value for the high pressure or low pressure coil, respectively.

The design of the experimental box model, as presented in Figure 12, includes holes at the top of one side of the baffle for the steam coolant outlet, and at the lower part of the other side of the baffle for the liquid coolant inlet. Insulating materials are employed to isolate the core from the inner surface of the box bottom, rendering the contact heat transfer between the iron core and the box shell negligible. Since the experimental model does not include core heating, the no-load loss and related calculations are omitted in the thermal circuit model computations of the experimental box. The box is filled with an evaporative coolant, submerging the core and coils. Several temperature measurement points are distributed near the upper flow channel of the coolant and approximately 2cm from the outer surface of the high-voltage coil in the lower layer. The temperature measurement points near the upper flow channel serve as evaporative coolant temperature nodes for monitoring purposes.

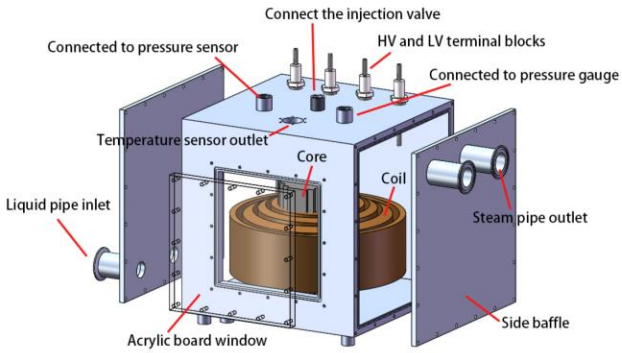

Figure 12. Experimental model of evaporative cooling transformer

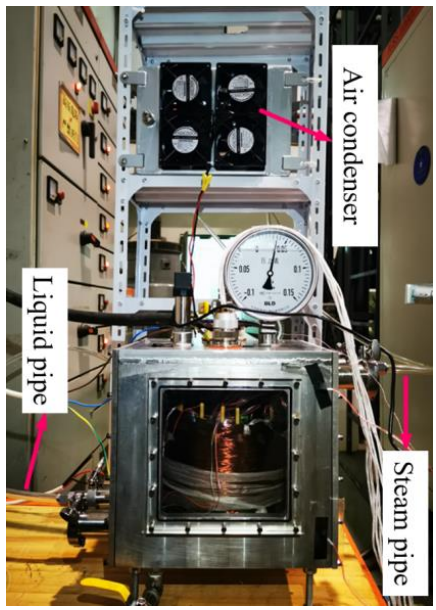

Figure 13. Experimental device

Figure 13 represents the experimental device. Prior to initiating the experimental process, it is essential to evacuate any residual air inside the box to negate potential impacts on condensation performance.

4.2 Selection of coolant for evaporative cooling

The selection of an appropriate evaporative coolant warrants the fulfillment of several conditions, including non-toxicity, environmental friendliness, non-flammability, non-explosiveness, and insulating performance. In addition to these, the coolant must demonstrate chemical compatibility with the varied materials housed within the transformer box. The boiling point of the chosen coolant must assure its residence within the nucleate boiling stage at the rated operational temperature of the transformer.

Taking into consideration the operating temperature characteristics of the transformer and the necessities of application scenarios, a novel type of fluorocarbon evaporative coolant has been identified, possessing a boiling point of 80℃ and an Ozone Depletion Potential (ODP) value of 0.

Table 1 compares the physical, chemical, and electrical performance parameters between this evaporative cooling fluid and commonly used insulating cooling fluids such as transformer oil.

Table 1. Performance comparison of selected fluorocarbon coolant and other insulating coolants

Parameter	I-10℃ Transformer Oil	The Fluorocarbon Coolant
Breakdown voltage [kV/2.5 mm]	60	53.9
Boiling point [℃]	-	80
Density [g/cm3]	0.86	1.69
Kinematic viscosity [mm2/s]	16	0.97
Specific heat (liquid) [kJ/(kg·℃)]	1.89	1.225
Latent heat of vaporization [kJ/kg]	-	85.8
Thermal conductivity [W/(m·K)]	0.131	0.064
Remarks	Measured at 25℃,1 atm	

From the data presented in Table 1, it is observed that while the breakdown voltage and specific heat capacity of the chosen evaporative coolant are marginally lower than that of transformer oil, its kinematic viscosity is notably less. This attribute implies that the heat transfer cycle of the fluorocarbon coolant is quicker than that of transformer oil. Moreover, the substantial latent heat of vaporization enables a stronger heat exchange capacity than that of transformer oil.

The physical property parameters of the fluorocarbon evaporative coolant, presented as a function of temperature, are represented in Eq. (30).

$$\begin{cases} \rho_{\mathrm{clt}} = 1752 - 2.46\theta_{\mathrm{clt}} \\ C_{\mathrm{clt}} = 1197.4 + 1.0911\theta_{\mathrm{clt}} \\ \lambda_{\mathrm{clt}} = 0.0691 - 0.0002\theta_{clt} \\ \alpha_{clt} = 0.00007 \\ \mu_{clt} = 0.0019\text{-}0.00001\theta_{clt} + 0.00000004\theta_{clt}^2 \end{cases} \tag{30}$$

In Eq. (30), the function *f(P)* is associated with the physical properties parameters of the coolant. The fitted relationship between the boiling point temperature $\theta_{clt\text{-}bp}$ (within a range of 40-110℃) and absolute pressure p (spanning from 18.8kPa to 259.8kPa) for the chosen evaporative coolant is represented as follows:

$$\theta_{clt-bp} = -90.69e^{-\frac{p}{120.83}} + 119.3 \tag{31}$$

4.3 Empirical analysis of the thermal circuit parameter of nucleate boiling heat transfer

An empirical investigation on the boiling heat transfer coefficient was conducted under constant pressure conditions. The correlation between the nucleate boiling heat transfer coefficient and heat flux density was extrapolated from numerous steady-state temperature rise experiments, which ranged load coefficients from K=0.5 to 2. The extrapolation is structured on the W. Rohsenow correlation, as depicted in Eq. (32). A value of 1.29 is adopted for the constant n1, which pertains to the surface of the heating element and the type of coolant, while the empirical coefficient Cwl, relative to the conjunction of the coil surface and coolant, is determined as 0.0078.

$$h_{\_zflq} = \frac{C_{p-l}}{0.0078r}\left[\frac{1}{\mu_l r}\sqrt{\frac{\sigma}{g(\rho_l-\rho_v)}}\right]^{-0.33}\left[\frac{C_{p-l}\mu_l}{\lambda_l}\right]^{-1.29} q_{\_rlmd}^{0.67} \tag{32}$$

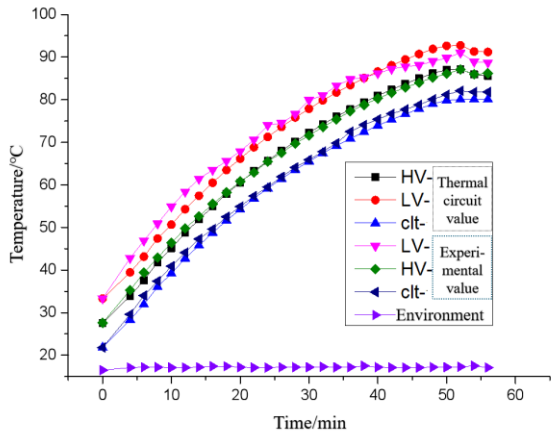

Figure 14. Comparison between the dynamic temperature rise experimental value and the calculated thermal circuit model value under rated load

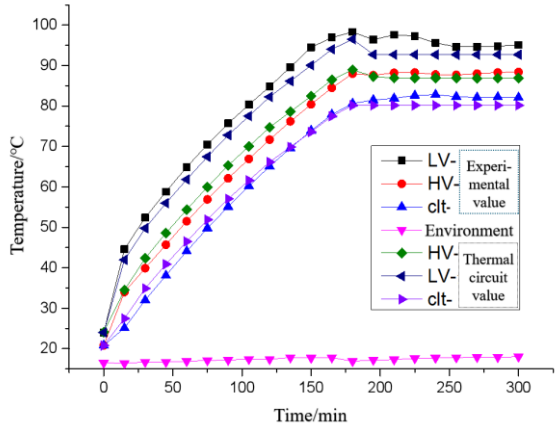

Figure 15. Comparison between the dynamic temperature rise experimental value and the calculated thermal circuit model value under K=1.2 load factor

A comparison of the thermal path model with multiple sets of dynamic temperature rise experimental results established the threshold value Δs of superheat degree in nucleate boiling heat transfer in the thermal circuit to be 7K. This value aligns well with the empirical findings. The average discrepancy between the multitude of experimental values and thermal circuit calculation values is roughly 5%, with the maximum relative error not exceeding 10%. Figures 14 and 15 illustrate comparisons between the empirical values and the calculated values of the thermal circuit model at the rated load and 1.2 times the rated load, respectively.

In both figures, it is observed that a minor sharp decline occurs concurrently in the temperature of the high and low voltage coils when the temperature of the evaporative coolant reaches the boiling point. Following this sharp decline, the temperature appears to stabilize. Before the coolant reaches the boiling point temperature, the temperature of the coils remains higher, even though the superheat degree of the coils' outer surface surpasses the threshold value Δs, as it still resides in the natural convection stage. Upon reaching the boiling point, the coolant immediately transitions from the natural convection stage to the nucleate boiling stage, causing the convection coefficient to rapidly increase and subsequently induce a sudden temperature drop on the outer surface of the coils.

5. THERMAL MODEL ANALYSIS AND PROTECTION

5.1 Association between load coefficient, hotspot temperature, and insulation grade

Figure 16 presents the dynamic temperature rise curve of the thermal circuit model under varying load conditions, crafted to emulate intermittent loads (i.e., loads necessitating frequent cold starts) common in industrial logistics parks. The coil's hotspot temperature is observed to attain its maximum value at the transition point when the heat transfer stage shifts from natural convection to boiling heat transfer. As the load increases, the duration to reach the transition point in a cold state decreases. Concomitantly, a higher load is associated with an elevated hotspot temperature at the transition point and a steeper gradient of the coil temperature at the transition from natural convection to boiling heat transfer.

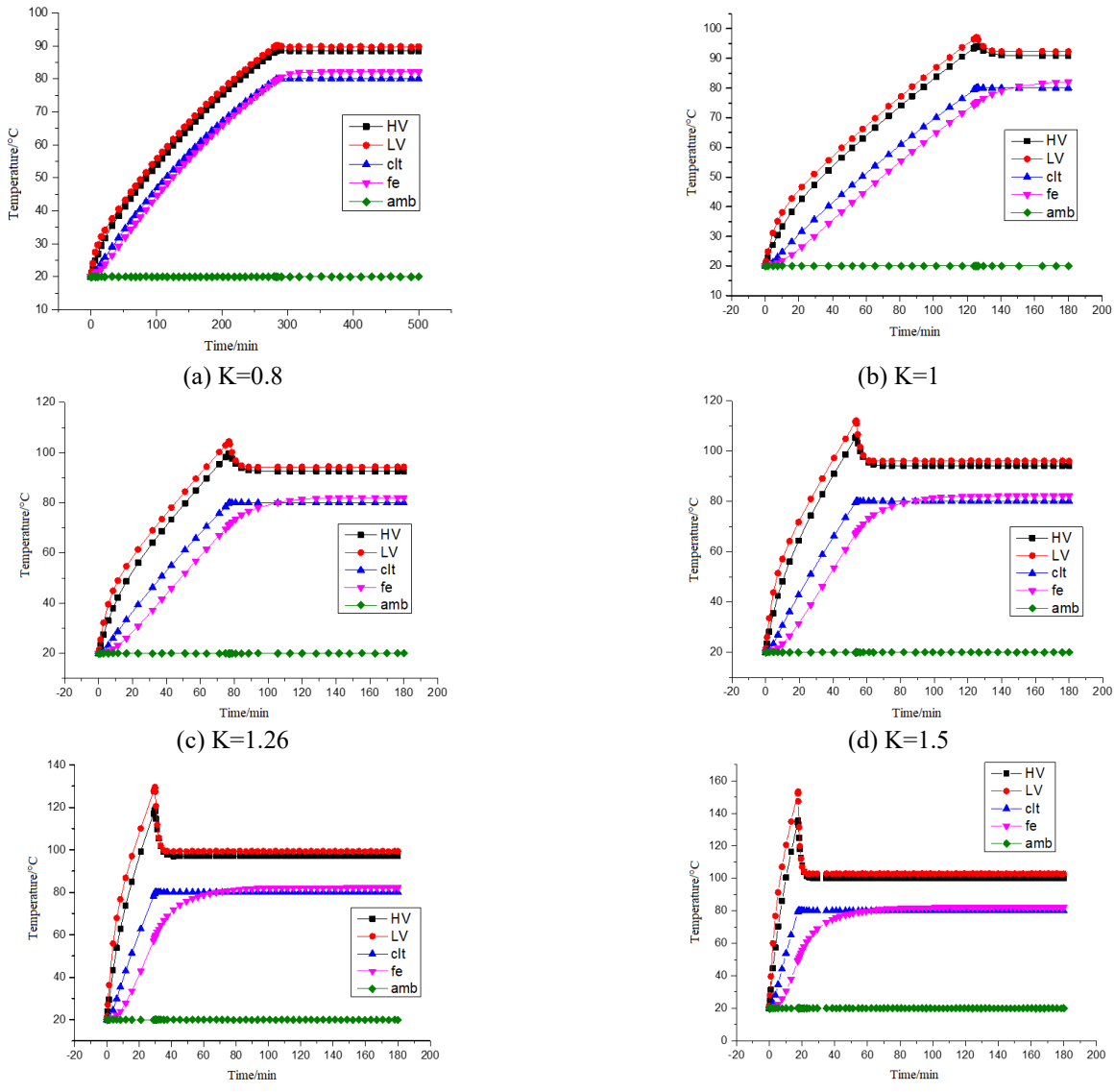

(a) K=0.8 (b) K=1

(c) K=1.26 (d) K=1.5

(e) K=2 (f) K=2.6

Figure 16. Dynamic temperature calculation value of thermal circuit model of prototype under different load conditions

Calculations reveal that no abrupt drop from natural convection to the transition stage occurs below a K=0.8 load factor. This suggests that under this load multiple, even when the coolant temperature reaches the boiling point, the temperature gradient between the outer surface of the winding and the surrounding coolant might not meet the threshold value Δs required for nucleate boiling initiation, thereby remaining within the natural convection stage. Alternatively, the threshold value Δs of nucleate boiling initiation might be reached, but due to an excessively small heat flux density, the boiling heat transfer coefficient approximates the natural convection heat transfer coefficient. Thus, when the evaporative coolant temperature meets the boiling point, the coil's hotspot temperature remains stable in the boiling heat transfer stage.

5.2 Ambient and operating temperature interplay

The impact of the ambient temperature on the dynamic temperature elevation curve was assessed via the thermal circuit model, revealing pertinent insights, as depicted in Figure 17. It becomes apparent that a decrease in the ambient temperature notably shortens the time necessary to reach the transition point. However, the ambient temperature does not influence the steady-state hotspot temperature value nor the peak hotspot temperature. This observation underpins the advantages of evaporative cooling transformers in high-temperature environments or during the summer months when compared to traditional transformers reliant on specific heat exchange.

5.3 Boiling point selection and operating characteristics

The association between the boiling point and the operating characteristics was analysed using four evaporative coolants - with boiling points of 47.6℃, 55℃, 80℃, and 110℃ - under the assumption of identical physical parameters and an ambient temperature of 20℃. The dynamic temperature elevation curve for a cold start is displayed in Figure 18. It is evident that, despite identical physical parameters, varying boiling points dictate different hotspot temperature values. This underlines the significance of the boiling point selection process. In the event that a transformer utilizes forced cooling in the condenser (owing to natural convection necessitating an increased vapour temperature at the secondary condensation side), possesses a low insulation level, and regularly operates under overload conditions, it is recommended to select an evaporative coolant with a low boiling point, as this facilitates the control of the hotspot temperature.

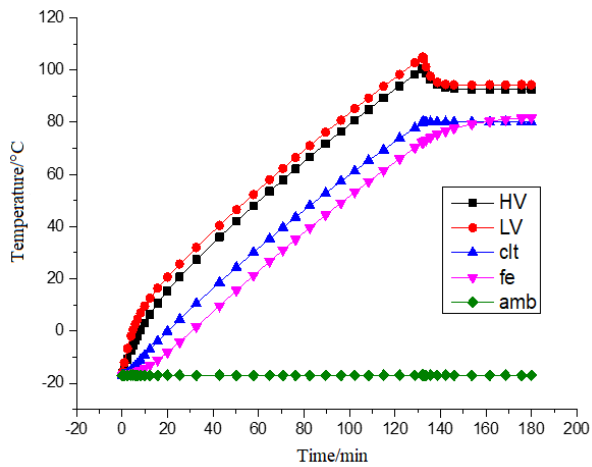

(a) θ_{amb}=-17℃

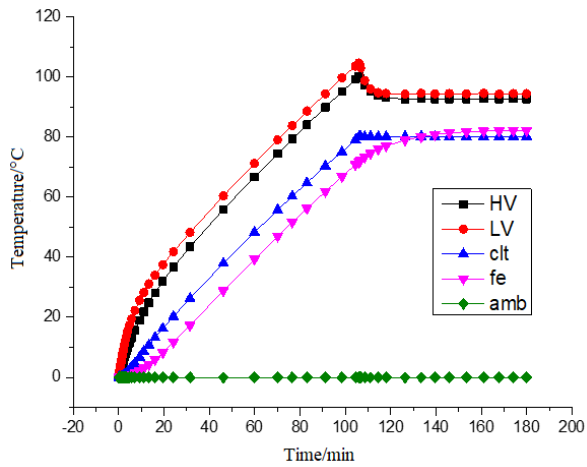

(b) θ_{amb}=0℃

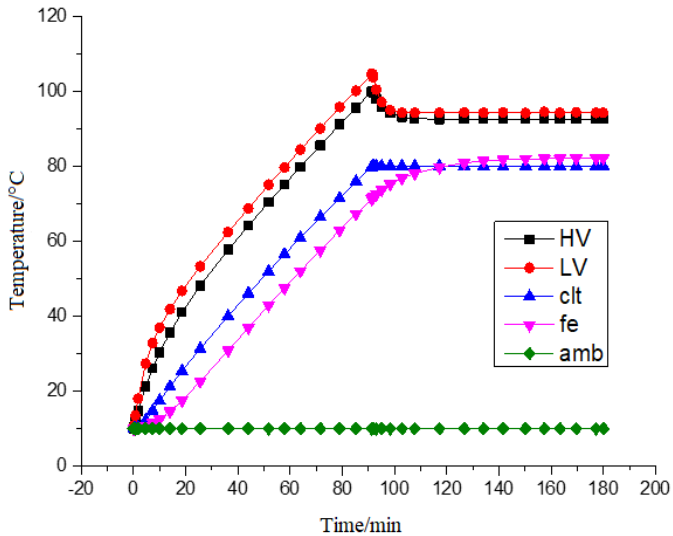

(c) θ_{amb}=10℃

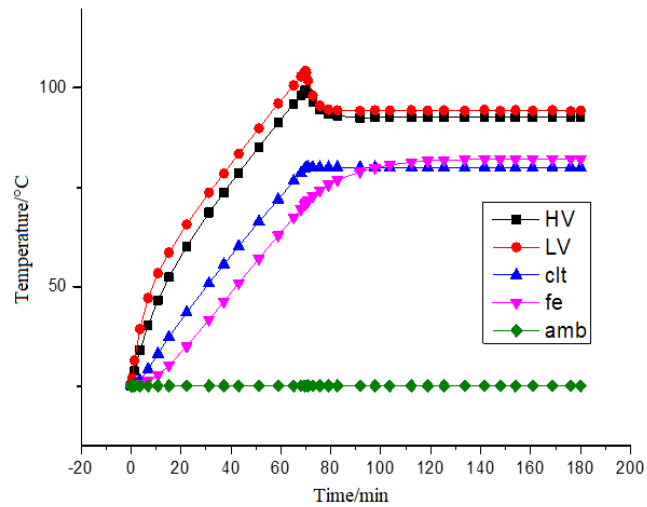

(d) θ_{amb}=25℃

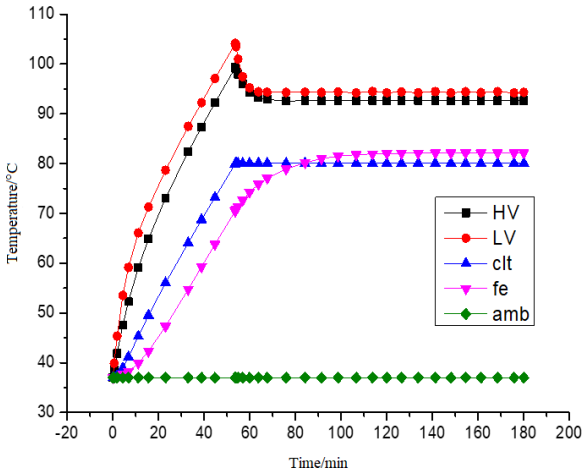

(e) θ_{amb}=37℃

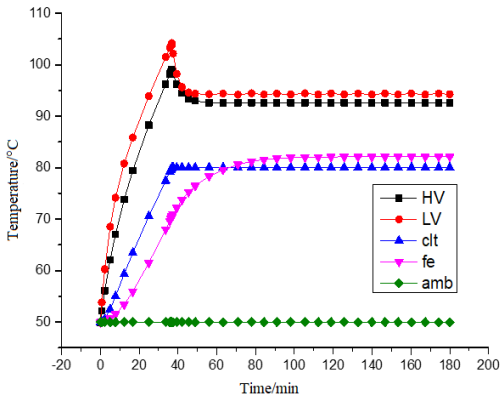

(f) θ_{amb}=50℃

Figure 17. Dynamic temperature elevation curves at varying ambient temperatures

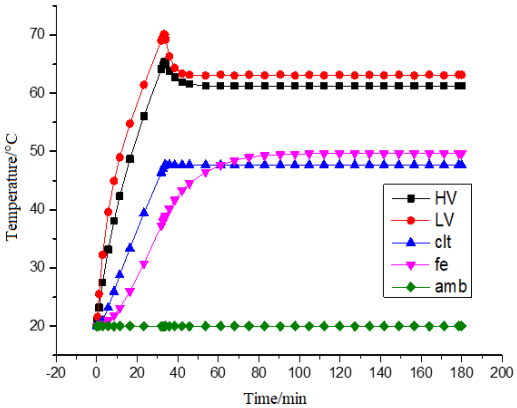

(a) boiling point θ_{bp}=47.6℃

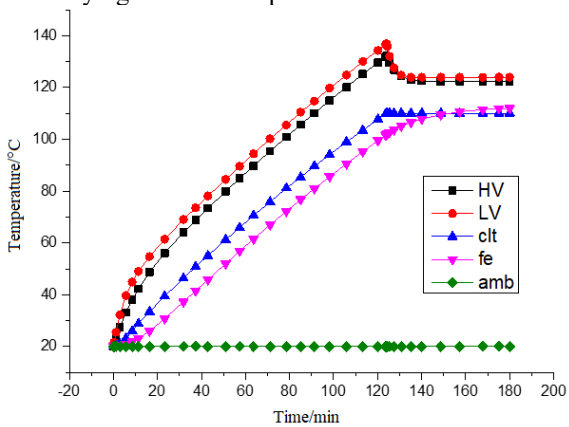

(d) boiling point θ_{bp}=110℃

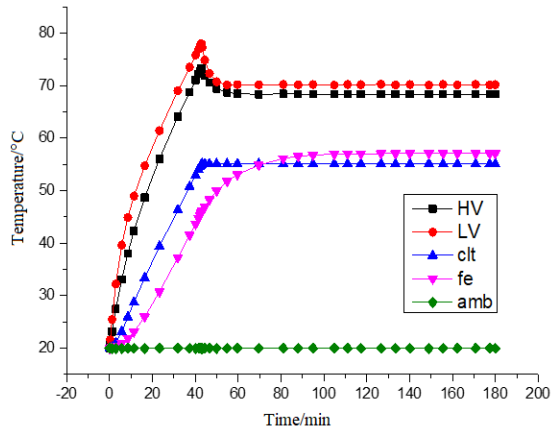

(b) boiling point θ_{bp}=55℃

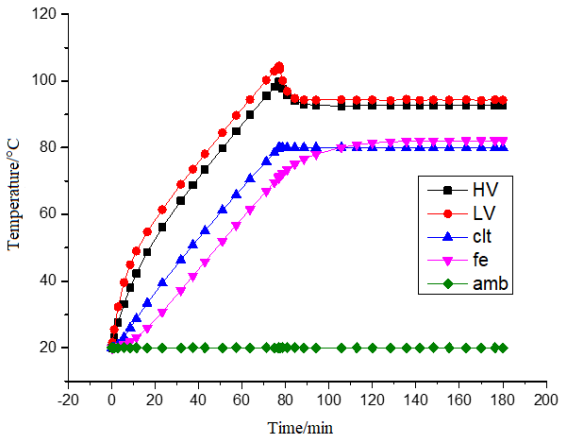

(c) boiling point θ_{bp}=80℃

Figure 18. Dynamic temperature rise curve of evaporative cooling coo lant with different boiling points

5.4 Mitigation and thermal protection of peak hotspot temperature at transition point

The preceding analysis underscores that as the load factor exceeds 0.8, an uptick in the load factor is accompanied by a more considerable hotspot temperature at the transition from natural convection to boiling heat transfer, along with a steeper temperature gradient from this transition point to the boiling heat transfer. The thermal circuit model's temperature elevation curve, as presented in Figure 19 (a), reveals that the elevated transition point temperature can be ascribed to the fact that under heavy loads, the evaporative coolant doesn't reach the boiling point, facilitating only single-phase convection for heat transfer between the coil and evaporative coolant, thus resulting in a lower heat transfer coefficient. Consequently, a high temperature gradient persists between the coil and evaporative coolant. Once the boiling point is reached by the evaporative coolant, the coil's superheat degree satisfies the nucleate boiling conditions, resulting in an improved heat transfer performance due to a large boiling heat transfer coefficient, leading to a sharp temperature drop in the coil, swiftly transitioning to the steady-state phase.

In the context of starting conditions within the boiling heat transfer stage, the most effective method to bypass this steep temperature drop is to satisfy nucleate boiling conditions before the coil reaches the steady-state hotspot temperature, essentially advancing to the nucleate boiling stage via

preheating. As an illustration, with a load factor K=7, the temperature elevation curve for transformers under impact loads, such as motor startup and rotor lockup, is simulated using cold start and preheating start methods respectively. Figure 19 (a) exhibits the dynamic temperature rise curve of a cold start loading seven times the impact load at an ambient temperature of 20℃, peaking at a hotspot temperature of 355.3℃ at the transition point. Conversely, Figure 19 (b) displays the dynamic temperature elevation curve of the impact load after reaching the rated operating temperature through preheating, recording a peak hotspot temperature of only 123.2℃ at the transition point. The temperature rise curve also indicates that transformers utilizing the immersed evaporative cooling topology showcase robust impact resistance load performance, with a significantly superior overload capacity compared to oil-immersed self-cooling distribution transformers dependent on single-phase convective heat transfer with specific heat.

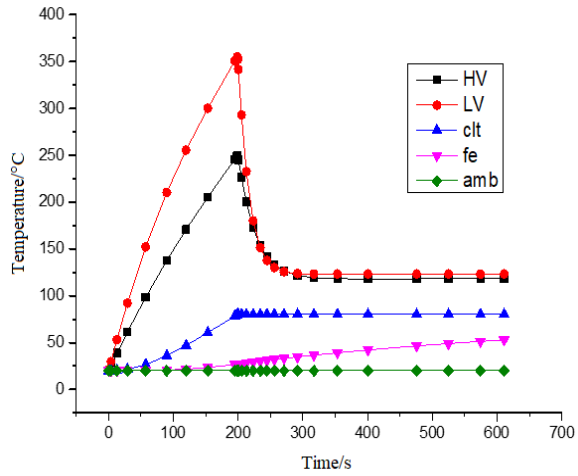

(a) Cold start load K=7 impact load

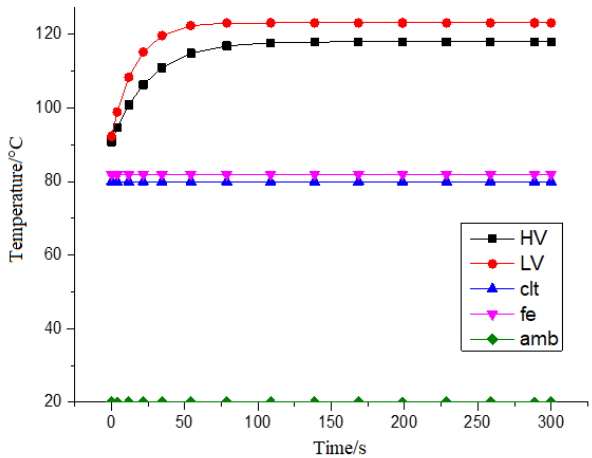

(b) Rated load load K=7 impact load

Figure 19. Dynamic temperature rise process of impact load under different starting modes

In conclusion, the optimal starting methodology entails initial preheating under conditions not exceeding the rated load, followed by loading the corresponding overload multiple upon reaching the nucleate boiling steady-state stage. This procedure effectively mitigates the high hotspot temperature value at the transition point, accomplishes the thermal protection objectives of the evaporative cooling transformer, and capitalizes fully on the superior overload resistance offered by the immersion evaporative cooling method.

6. CONCLUSIONS

The present study investigated the prevalent issue of overload in distribution transformers, centering its focus on the convective thermal resistance in the thermal circuit of existing distribution transformers. The research pursued the improvement of heat dissipation capacity, guided by an analysis of thermal circuit parameters. The process of optimizing the internal and external thermal resistance of the transformer's thermal circuit, employing evaporative cooling technology, was examined through a synergistic approach of theory and experimental data.

A dynamic thermal circuit model of a multi-stage immersed evaporative cooling transformer, capable of reflecting single-phase natural convection and two-phase boiling heat transfer, was established, guided by the subsection characteristics of the boiling heat transfer curve of a low boiling point coolant. The liquid coolant temperature served as the controlled source for pressure parameter control. A comprehensive analysis was carried out on thermal circuit parameters, critical heat flux density limits, and the characteristics of evaporative coolant. Correlations of nucleate boiling heat transfer for the chosen evaporative coolant were derived through model tests at varying heat flux densities.

The study also assessed the influence of factors such as load coefficient, coolant boiling point, and environmental temperature on operating characteristics. Additionally, the eradication of the peak hotspot temperature at the transition point and thermal protection were evaluated. The study demonstrated that immersed evaporative cooling transformers significantly augment overload resistance performance, making them especially suitable for impact, intermittent, and fluctuating loads. Such transformers hold vast potential for implementation in settings like industrial logistics parks.

This research contributes valuable insights for the theoretical understanding, calculation, design, operation, and production of evaporative cooling technology deployed in distribution transformers. However, the heat flux level of the evaporative coolant used in the evaporative cooling transformer model experiment was relatively low. This low level results in a certain deficit in heat transfer performance in comparison to other evaporative cooling methods, such as cold plate liquid box and tube cooling. This discrepancy can be attributed to the lack of comprehensive research on the boiling heat transfer characteristics of narrow channel self-circulation flow relative to cold plate and tube cooling. Future research should concentrate on the outer surface of evaporative cooling transformer coils and confined areas like flow channels. Investigations should aim to amplify the formation of bubbles through physical or structural modifications to further enhance the boiling heat transfer performance of the evaporative cooling transformer.

REFERENCES

[1] Fu, H., Yang, X.L., Zhang, B., Wang, Q., Qu, M.R. (2020). Analysis of transformer thermal life loss considering large-scale new energy resources access. Journal of Electric Power Science and Technology, 35(6):

53-60. https://doi.org/10.19781/j.issn.1673-9140.2020.06.007
[2] Gu, G.B., Ruan, L., Liu, F.H., Xiong, B. (2015). Development, application, and prospects of evaporative cooling technology. Transactions of China Electrotechnical Society, 30(11): 1-6.
[3] Gu, G.B., Ruan, L. (2014). Application and developments of evaporative cooling technology in the field of hydrogenerators. Proceedings of the CSEE, 34(29): 5112-5119.
[4] Guo, J.H., Gu, G.B., Fu, D.P., Huang, D.S. (2013). Cooling characteristics and performance of the 330MW evaporative cooling turbo generator. Transactions of China Electrotechnical Society, 28 (3): 134-139.
[5] Guo, H., Song, F.C., Yuan, J.Y., Li, S.K. (2006). The research of the evaporative cooling electromagnetic iron-separater. Proceedings of the CSEE, 2006(11): 60-64.
[6] Li, Z.G., Tian, X.D., Zhang, G.Q., Gao, W.N. (2008). Evaporative cooling technology applied to inverter of power plant air-cooling fan. Electric Power Automation Equipment, 2008 (10): 116-119. https://doi.org/10.3969/j.issn.1006-6047.2008.10.028
[7] Shi, H.L., Xiong, B., Liu, Z.K., Jia, Y.Y., Gu, G.B. (2021). Research on phase change heat dissipation of high voltage inverter power module. Advanced Technology of Electrical Engineering and Energy, 40(6): 73-80. https://doi.org/10.12067/ATEEE2012021
[8] Xiong, B., Ruan, L., Gu, G.B. (2016). Development of high power density evaporative cooling magnet coils in ECR ion source. Electric Machines and Control, 20(1): 22-28. https://doi.org/10.15938/j.emc.2016.01.004
[9] Guo, S.Q., Ruan, L., Li, Z.G., Liu, F.H. (2013). The design of controlling system in the evaporative cooling super computer simulation experiment platform based on PLC. Applied Mechanics and Materials, 437: 734-739. https://doi.org/10.4028/www.scientific.net/AMM.437.734
[10] Ruan, L., Zhenguo, L. (2012). The discussion of energy conservation of data center from the evaporative cooling technology of HPC. In Proceedings of the International Conference on Parallel and Distributed Processing Techniques and Applications (PDPTA). The Steering Committee of The World Congress in Computer Science, Computer Engineering and Applied Computing (WorldComp), 584-589.
[11] Niu, W.H. (2016). Research of key technologies of nonflammable fluorocarbon immersed power transformer. University of Chinese Academy of Sciences, 2016.
[12] Nukiyama S. (1934). Film boiling water on thin wires. Society of Mechanical Engineering, 37: 367-374.
[13] Lv, J.F., Wu, Y.X., Li, Z.H., et al. (2017). Vapor-liquid two-phase flow and boiling heat transfer. Beijing: Science Press, 2017.
[14] Rohsenow, W.M. (1952). A method of correlating heat-transfer data for surface boiling of liquids. Transactions of the American Society of Mechanical Engineers, 74(6): 969-975. https://doi.org/10.1115/1.4015984
[15] Yang, C.X., Wu, Y.T., Yuan, X.G., Ma, C.F. (1999). Dynamic characteristics of bubble growth and departure in nucleate boiling-Bubble departure diameter and frequency. Journal of Engineering for Thermal Energy and Power, 1999 (5): 330-333, 408.
[16] Chen, Z.B. (1975). Strengthening of the evaporative cooling process of the motor coil by different insulation materials. Large Electric Machine and Hydraulic Turbine, 1975(4): 22-26.
[17] Luan, R. (2004). Research on insulation and heat-transfer system of stator in evaporative cooling horizontal electrical machine. Graduate School of Chinese Academy of Sciences (Institute of Electrical Engineering).
[18] Deng, B. (2002). The evaporative cooling transformer experimental research and analysis. Hebei University of Technology.
[19] Song, M.K. (2015). Experimental research on heat-transfer performance of evaporative cooling transformer. Hebei University of Technology.
[20] Zhao, W. (2014). The research and analysis on evaporating cooling transformer windings temperature field and flow field. Hebei University of Technology. https://doi.org/10.7666/d.D757491
[21] Zhao, W., Liu, J.Q., Zhang, C.W., Chai, S.Y., Wang, X.C. (2016). Operation condition research on an evaporative cooling transformer. Transformer, 53(11): 34-37.
[22] Zhang, C.W. (2015). Numerical design and numerical simulation of the new evaporative cooling transformer. Hebei University of Technology.
[23] Zuber, N. (1958). On the stability of boiling heat transfer. Transactions of the American Society of Mechanical Engineers, 80(3): 711-714.

NOMENCLATURE

Symbol Table

q	Heat flux, W
Re	Reynolds number
h	Convective heat transfer coefficient, $W/(m^2 \cdot K)$
Nu	Nusselt number
D	Departure diameter, m
Pr	Prandtl number
A	Area, m^2
Gr	Grashof number
c	Specific heat capacity, $J/(kg \cdot K)$
r	Latent heat, J/kg
g	Gravitational acceleration, m/s^2
p	Pressure, Pa
Rth	Thermal resistance, K/W
m	Mass, kg
δ	Thickness, m
$q_{\_rlmd}$	Heat flux density, W/m^2
α	Expansion coefficient of fluid, K^{-1}
μ	Dynamic viscosity, Pa•s
ρ	Density, kg/m^3, kg/m^3
θ	Celsius temperature, ℃
λ	Thermal conductivity, $W/(m^2 \cdot K)$
σ	Surface tension, N/m

Subscripts

hs	winding hot spot
amb	environment
LV	low-voltage winding
HV	high-voltage windin
l	liquid phase
v	vapor state

zflq	evaporative coolant	w	wall
boil	boiling heat transfer	bp	boiling point
fe	core	s	saturated state of system in boils
clt	coolant		